Title

Synchronization of Geodesic Acoustic Modes and Magnetic Fluctuations in Toroidal Plasmas

Journal

Physical Review Letters, 117(14)

ISSN

0031-9007

Authors

Zhao, KJ
Nagashima, Y
Diamond, PH
et al.

Publication Date

2016-09-30

DOI

10.1103/physrevlett.117.145002

Synchronization of Geodesic Acoustic Modes and Magnetic Fluctuations in Toroidal Plasmas

K. J. Zhao,[1,*] Y. Nagashima,[2] P. H. Diamond,[3] J. Q. Dong,[1,4] K. Itoh,[5] S.- I. Itoh,[2] L. W. Yan,[1] J. Cheng,[1] A. Fujisawa,[2] S. Inagaki,[2] Y. Kosuga,[2] M. Sasaki,[2] Z. X. Wang,[6] L. Wei,[6] Z. H. Huang,[1] D. L. Yu,[1] W. Y. Hong,[1] Q. Li,[1] X. Q. Ji,[1] X. M. Song,[1] Y. Huang,[1] Yi. Liu,[1] Q. W. Yang,[1] X. T. Ding,[1] and X. R. Duan[1]

[1]*Southwestern Institute of Physics, P.O. Box 432, Chendu 610041, China*
[2]*Research Institute for Applied Mechanics, Kyushu University, Kasuga, Kasuga koen 6-1, 816-8580, Japan*
[3]*Center for Momentum Transport and Flow Organization, University of California at San Diego, California, San Diego 92093, USA*
[4]*Institute for Fusion Theory and Simulation, Zhejiang University, Hangzhou 310027, China*
[5]*National Institute for Fusion Science, Toki 509-5292, Japan*
[6]*School of Physics and Optoelectronic Technology, Dalian University of Technology, Dalian 116024, China*

(Received 10 March 2016; revised manuscript received 13 June 2016; published 28 September 2016)

The synchronization of geodesic acoustic modes (GAMs) and magnetic fluctuations is identified in the edge plasmas of the HL-2A tokamak. Mesoscale electric fluctuations (MSEFs) having components of a dominant GAM, and $m/n = 6/2$ potential fluctuations are found at the same frequency as that of the magnetic fluctuations of $m/n = 6/2$ (m and n are poloidal and toroidal mode numbers, respectively). The temporal evolutions of the MSEFs and the magnetic fluctuations clearly show the frequency entrainment and the phase lock between the GAM and the $m/n = 6/2$ magnetic fluctuations. The results indicate that GAMs and magnetic fluctuations can transfer energy through nonlinear synchronization. Such nonlinear synchronization may also contribute to low-frequency zonal flow formation, reduction of turbulence level, and thus confinement regime transitions.

DOI: 10.1103/PhysRevLett.117.145002

The interaction of magnetic field structures and flows in magnetohydrodynamics is a subject of general interest in physics. Typical examples include magnetic braking of stellar rotation [1], angular momentum transport in astrophysical disks [2,3], and the dynamics of Earth's core and geodynamo [4]. In fusion plasmas, the interactions between plasma flows and magnetic fluctuations have attracted attention for understanding and control of plasma confinement and transport. For example, the neoclassical tearing modes, which need a seed magnetic island for onset [5,6], can be, theoretically, triggered by a turbulence noise source [7]. At the same time, the magnetic island-induced sheared flows can suppress turbulence and contribute to the formation of an internal transport barrier [8]. The coupling of toroidal Alfvén eigenmodes (TAEs) and Beta-induced Alfvén eigenmodes (BAEs) to the zonal flows is predicted to reduce the saturation level of TAEs and BAEs so as to reduce fast ion loss [9]. For the mitigation or suppression of the large edge localized modes in the high confinement mode (H-mode) plasmas, which is considered to be an urgent task for fusion research, the resonant magnetic perturbations (RMPs) [10] are used worldwide. In applying RMPs, the interactions of magnetic perturbations, zonal flows [11], and microscopic turbulence take place.

Two types of zonal flows, i.e., the low-frequency zonal flows (LFZFs) [11,12] and the geodesic acoustic modes (GAMs) [13,14], are known. The effects of magnetic perturbation on zonal flows were reported. For instance, the GAM is damped in the presence of RMPs [15]; the RMP-induced magnetic islands can enhance the LFZFs and turbulence at their boundary [16]; the poloidal flows are reversed when the RMP-induced island width is large enough [17]; a quasicoherent mode is detected near the low safety factor rational surface [18,19]. However, the dynamical and mutual interaction between flows and magnetic perturbations has not been deeply studied experimentally.

To understand the complicated interaction of the flows with the magnetic structures, we have to know the ways of their interaction dynamically. Here, the first observation of the synchronization, a universal nonlinear phenomenon in nature [20–23], of GAMs and magnetic fluctuations in the edge plasmas of the HL-2A tokamak is reported. The frequency entrainment and phase lock, two essential elements in synchronization, are demonstrated. Because the magnetic field and velocity field are the two essential vector fields in plasmas, governing the turbulent structure formation in the Universe and laboratory, the discovery of synchronization reveals a new, essential, and prototypical process in the nonlinear dynamics of high-temperature plasmas.

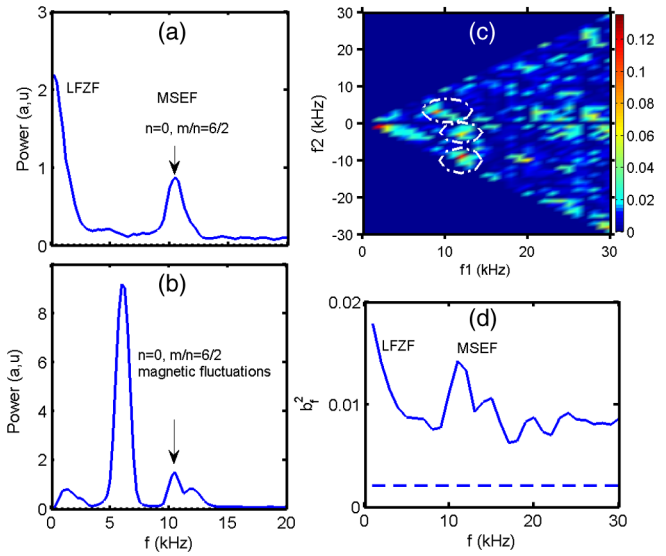

FIG. 1. The autopower spectra of the floating potential fluctuations (a), magnetic fluctuations (b), squared bicoherence (c), and total bicoherence (d).

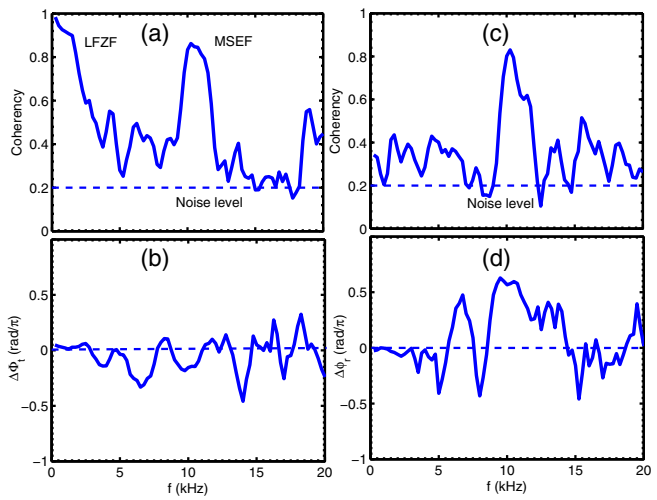

FIG. 2. (a) The toroidal coherency between potential fluctuations and (b) its phase shifts, (c) the coherency between the floating potential and magnetic fluctuations, and (d) the radial phase shifts between potential fluctuations.

The experiments presented here were conducted in Ohmic and electron-cyclotron-resonance-heating (ECRH) deuterium plasmas of a circular cross section on the HL-2A tokamak. The major and minor radii of the HL-2A tokamak are $R = 1.65$ m and $a = 0.4$ m, respectively. The ECRH power is ~500 kW. The parameters specially set for the experiments are the toroidal magnetic field $B_t = 1.2$–1.3 T, the plasma current $I_p = 150$–180 kA, the line-averaged electron density $\bar{N}_e = 1$–2×10^{19} m^{-3}, and the safety factor $q_a = 3.3$. The sampling rate of the probe data is 1 MHz, corresponding to a Nyquist frequency of 500 kHz. The frequency resolution is 0.25 kHz in the following analysis unless otherwise stated. A combination of distributed Langmuir probe (LP) arrays was used to measure floating potential fluctuations and the Mach number. In the combination, a LP array of three tips and a four-tip LP array form a fast reciprocating probe set of seven tips with a 65 mm poloidal span. A radial rake probe array of 12 tips, in the toroidal direction, is located in the poloidal cross section ~2100 mm away from the set of seven tips. It was used to get profiles of floating potential fluctuations. The tip size and the mount of the LP sets are the same as was described in Ref. [24].

The mesoscale electric fluctuations (MSEFs) with components of the dominant GAMs and the $m/n = 6/2$ potential fluctuations are detected inside the last closed flux surface (LCFS) in ECRH plasmas. The tips are located at the radial position of $\Delta r = -4.6$ cm, where the minus sign means inwards from the LCFS. Figures 1(a) and 1(b) give the autopower spectra of the floating potential fluctuations and the magnetic fluctuations from the Mirnov coils set up on the vacuum vessel wall, respectively. The small peak shown in Fig. 1(a) at the frequency of ~10.5 kHz is the MSEF. A large power fraction peak of the LFZF in the frequency range of ~0.25–3 kHz is also detected. The large peak at the frequency of ~6 kHz shown in Fig. 1(b) is the tearing modes with mode numbers of $m/n = 2/1$. The small peak presented in Fig. 1(b) at the same frequency as the MSEFs has components of the dominant $m/n = 6/2$ magnetic fluctuations and the $n = 0$ zonal field. Besides, the two small peaks at the frequency of 1.2 and 12 kHz come from the power supply and the $m/n = 4/2$ tearing mode, respectively.

The interaction between LFZFs and MSEFs is an important physics mechanism associated with LFZF formation mechanism. The bicoherence analysis, an indicator for the strength of nonlinear three-wave coupling, can be used to prove the existence of the interaction between LFZFs and MSEFs. The squared autobicoherence $b_f^2 = |B(f)|^2/[\langle|\phi_f(f_1)\phi_f(f_2)|^2\rangle\langle|\phi_f(f)|^2\rangle]$ of the perturbations is calculated. Here the bispectrum $B(f) = \langle\phi_f(f_1)\phi_f(f_2)\phi_f^*(f = f_1 + f_2)\rangle$, while $\langle\ldots\rangle$ denotes an ensemble average. The frequency resolution is 1 kHz, the number of realization is $M = 472$, and the noise level is 0.002 for the analysis. Figure 1(c) plots the squared autobicoherence of the floating potential fluctuations in the low-frequency region of $f_1 < 30$ kHz, and $f_2 = -30 - +30$ kHz. The bicoherence in the frequency region (dash-dotted ellipse) of $f_1 = 9$–14 kHz, $f_2 = 0$–± 5 kHz, and $f = f_1 + f_2 = 0$–5 kHz is significantly above the noise level. This analysis suggests that the MSEFs may contribute to the LFZF formation through the nonlinear three-wave coupling between MSEFs and LFZFs. The total bicoherence is shown in Fig. 1(d). The peaks in the LFZF and MSEF frequency regions indicate that LFZFs and MSEFs can also interact with the turbulence.

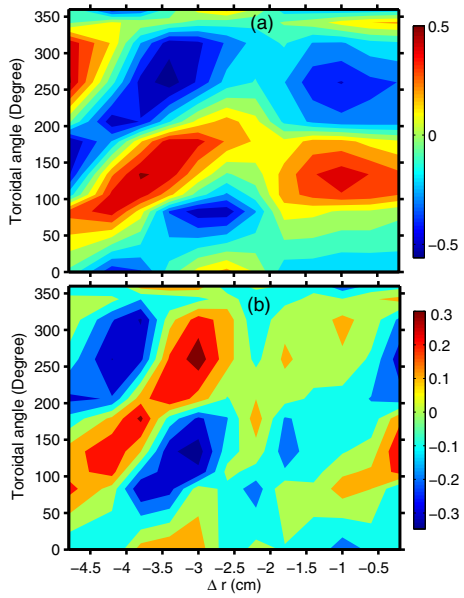

FIG. 3. The contour plots of coherency between the potential and magnetic fluctuations (a) and between the turbulence envelope and magnetic fluctuations in the frequency band of 9–11 kHz (b).

Figures 2(a)–2(d) show the toroidal coherency between potential fluctuations, their phase shifts, the coherency between the floating potential and magnetic fluctuations, and the radial phase shifts between potential fluctuations, respectively. The toroidal coherency in the LFZF and MSEF frequency bands is all quite high. This indicates that the MSEF and LFZF have a strong correlation in the toroidal direction with a span of 2100 mm. The corresponding phase shift in the MSEF frequency region is estimated as $\Delta\phi_t = 0.25 \pm 0.09$ rad. The toroidal mode number is calculated as $n = 0 \pm 0.2$. The evaluated radial phase shift is $\Delta\phi_r = 1.4 \pm 0.2$ rad, and the corresponding radial wave vector is estimated as $k_r = 3.5 \pm 0.2$ cm^{-1} with a span of 4 mm in the radial direction. Thus, we conclude that the MSEF has the characteristics of the toroidal symmetry and finite radial wave numbers, and thus the GAM component is dominant. In addition, the calculated coherency between the MSEFs and the magnetic fluctuations at the MSEF frequency is significantly above the noise level, indicating that the MSEFs are well correlated with the magnetic fluctuations.

The spatial structures of the MSEF at the frequency of ~10.5 kHz were identified with further correlation analysis. The coherency is described as $C_{XY} = \langle (X_i - X)(Y_i - Y)\rangle / [\sqrt{\langle (X_i - X)^2\rangle}\sqrt{\langle (Y_i - Y)^2\rangle}]$, where X_i and Y_i are two sets of variables, i stands for time series. The 12 probe tips are uniformly distributed in the radial direction from −4.8 to −0.4 cm inside the LCFS. The ten Mirnov coils are located at different toroidal angles. Combining the probe signals with the Mirnov signals, the 2D structures of the modes can be obtained, because the

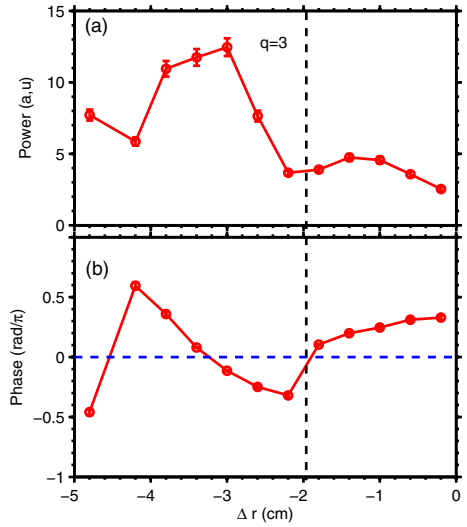

FIG. 4. (a) The radial profiles of MSEF power and (b) the phase shifts between the potential and magnetic fluctuations of $m/n = 6/2$.

C_{XY} contains the phase shift information. Figure 3(a) shows the contour of $C(X(\Delta r), Y(\xi))$, where $X(\Delta r)$ is the potential perturbation at $r = a + \Delta r$ and $Y(\xi)$ is the magnetic fluctuation measured with the Mirnov coil at the toroidal angle ξ. The toroidal mode number of $n = 2$ is clearly demonstrated for the potential fluctuation at the frequency of ~10.5 kHz. The poloidal mode number of $m = 6$ is also estimated with similar analysis. Figure 3(b) also gives the contour plot of the coherency between turbulence envelopes and magnetic fluctuations. Here, the turbulence envelope is calculated from the high-frequency fluctuations of >30 kHz through the Hilbert transform. The envelope can be described as $\sqrt{x_{(t)}^2 + y_{(t)}^2}$, where $x_{(t)}$ and $y_{(t)}$ are the real and imaginary parts of the analytic signal, respectively [25]. The poloidal and toroidal mode numbers for the turbulence envelope are identified as $m = 6$ and $n = 2$, respectively. This analysis indicates that the MSEF also contains $m/n = 6/2$ potential fluctuations. The phase shift between the turbulence envelope and the $m/n = 6/2$ potential fluctuation is close to $\pi/2$. The radial wavelengths of the $m/n = 6/2$ potential fluctuation and turbulence envelope are all estimated as about ~2 cm. The $m/n = 6/2$ potential fluctuation propagates in the directions of the toroidal magnetic field and ion diamagnetic drift.

The radial distributions of the potential fluctuation power at the MSEF frequency are measured and shown in Fig. 4(a). The power as a function of the radial position shows two peaks. The amplitude of the MSEF first increases from the LCFS inwards but reduces at the position of $\Delta r \sim -2.0$ cm, where the surface of the safety factor $q = 3$ is located. Then the power increases again and reaches a maximum at $\Delta r \sim -3.0$ cm. After that, the power deceases inwards. The profiles of the phase shift between the MSEFs and the

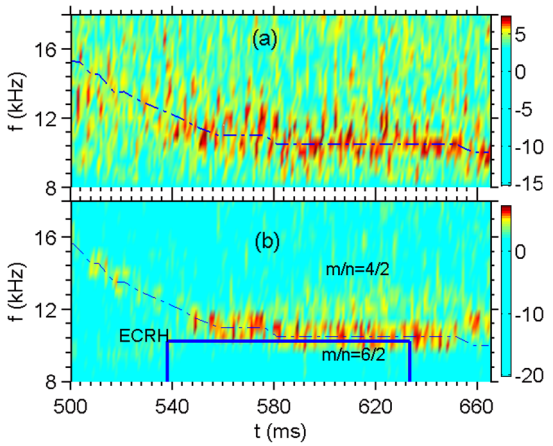

FIG. 5. The spectrograms of the MSEFs (a) and magnetic fluctuations of $m/n = 6/2$ (b) (the dash-dotted line indicates the evolution of the center of the MSEF frequency).

magnetic fluctuations by fast Fourier transformation analysis is also provided in Fig. 4(b). The sign of the phase shift changes at $\Delta r \sim -2.0$ cm, indicating that the sign of the MSEF inverts at the $q = 3$ surface. The reduction of the MSEF and the change of the sign for the MSEF around $q = 3$ surface may come from the $m/n = 6/2$ islands. The radius of the $q = 3$ surface is estimated by magnetic measurements.

In order to understand the interaction mechanism of the GAMs and the magnetic fluctuations, the temporal evolutions of the MSEFs and magnetic fluctuations of $m/n = 6/2$ are investigated. Figure 5(a) shows the spectrogram of the floating potential fluctuations in the MSEF frequency range at the radial position of $\Delta r = -3.0$ cm. In the period of 500–530 ms, the MSEF frequency rapidly decreases from 15.5 to 12.5 kHz. At the beginning of the ECRH heating, the MSEF is located at the frequency of ~12.5 kHz, and its frequency decreases continuously. After ~590 ms, the MSEF frequency becomes stable and is about 10.5 kHz. Figure 5(b) also gives the spectrogram of the $m/n = 6/2$ magnetic fluctuations. The $m/n = 6/2$ magnetic fluctuations follow the MSEF frequency, and its intensity increases gradually. At 20 ms after the ECRH switching off, i.e., at ~650 ms, the MSEF frequency decreases again and no significant magnetic fluctuation is observed at the MSEF frequency. The result suggests that the frequency entrainment of the GAM and the $m/n = 6/2$ magnetic fluctuations exists during the ECRH heating.

The phase lock is another important evidence to prove the frequency entrainment linked to the nonlinear synchronization of GAMs and magnetic fluctuations. Figure 6 shows the probability distribution function (PDF) of the phase shifts between MSEFs and magnetic fluctuations at different time slices. The phase shifts are estimated with the Hilbert transform. Before ECRH heating, the peaks are clearly shown in all time periods given here. After ECRH switching on, the peaks become stable and more significant, especially during the periods of 590–600 and 600–610 ms. This is consistent with the frequency entrainment observed during ECRH heating. After ECRH switching off, the half width of the peaks becomes wider and the peak disappears gradually. The analysis of the phase PDFs also shows that the significant peaks in PDFs during the ECRH appear always, while the apparent peaks in PDFs before ECRH appear or disappear shot to shot. This observation suggests that the phase shifts between GAMs and magnetic fluctuations can be locked through adjusting their phases via a nonlinear interaction during the ECRH heating.

This experiment is designed to measure the mode numbers of GAMs ($n = 0$) and potential fluctuations ($m/n = 6/2$) with the same frequency and the radial distribution of the MSEFs simultaneously and performed with multiple discharges and with similar plasma parameters. For this analysis, 20 shots have been used, among

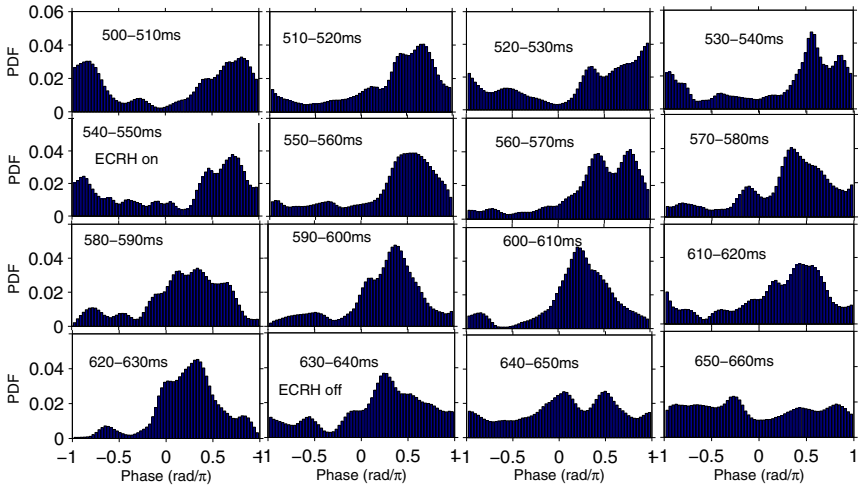

FIG. 6. The probability distribution functions of phase shifts between MSEFs and magnetic fluctuations at different time slices.

which 17 shots show such a phenomenon unambiguously. The $m/n = 3/1$ basic harmonic mode is not observed in the present experiments. This indicates that the $m/n = 6/2$ mode does not come from the $m/n = 3/1$ basic harmonic mode. The turbulence-driven GAMs has a close frequency with $m/n = 6/2$ magnetic fluctuations. The synchronization of GAMs and magnetic fluctuations suggests that GAMs and magnetic fluctuations can transfer energy between each other through nonlinear synchronization. Therefore, the observation suggests that synchronization might contribute to the excitation of $m/n = 6/2$ magnetic fluctuations. This cannot be understood by the present theory. In this experiment, we also observed that the MSEFs interact with LFZFs and turbulence, suggesting that the synchronization contributes to the LFZF formation and, thus, reduces the turbulence level. The LFZF is favorable for the low to high confinement mode (L-H) transitions. Thus, we speculate that the synchronization can contribute to confinement regime transitions, especially L-H transitions. Note that the $m/n = 4/2$ mode of $f \sim 12$ kHz is not correlated with GAMs. The possible conjecture is that the $q = 2$ rational surface is far away from the GAM location, although the $m/n = 4/2$ mode frequency is close to that of GAMs. The $m/n = 4/2$ modes occur at the $q = 2$ rational surface in the core plasmas, while both the GAMs and the $m/n = 6/2$ modes are localized in the edge plasmas. This difference between $4/2$ and $6/2$ modes gives a clue to understand the mechanism that causes observed synchronization.

In summary, synchronization of GAMs and magnetic fluctuations is observed for the first time in the edge plasmas of the HL-2A tokamak using multiple Langmuir probe arrays. This is the discovery of the new and essential structure formations of plasmas, in which the two fundamental vector fields (magnetic field and flow field) couple dynamically.

The theoretical explanation of this observation is left for future studies. However, this observation shows the importance of its own, because it provides a problem definition to study nonlinear interactions among magnetic islands and the low-frequency zonal flows and GAMs. It has been theoretically pointed that the mean and zonal flows and magnetic island interact directly; e.g., the influence of the flow on island growth [26] and that by a magnetic island on flow [27] have been reported. The indirect interactions between flows and islands have also been extensively studied. Here, indirect means the interaction between them via a change of turbulence. That is, the energy of microscopic turbulence is transferred to the tearing mode [28,29], so that the fluctuation intensity and the drive of zonal flows by turbulence can be reduced. The magnetic islands enhance the damping rate of zonal flows, so that they affect the intensities of flows and turbulence simultaneously [30]. These theoretical studies have focused on the impacts, which are given as averaged values on the magnetic surface, so that the sensitivity to the phase of a magnetic perturbation has not attracted much attention. It has also been pointed out that the fluctuation intensity is modulated with the same period as magnetic islands [28,29], and an initial observation was reported [31]. Therefore, there can be a coupling effect between them, which is sensitive to the phase of the magnetic island. The fact that the zonal flow is synchronous with the island actually suggests that the zonal flows see the islands and respond to the island with sensitivity to the phase. Thus, we emphasize that this is indeed an important contribution to the expanding subject of how magnetic structures and transport can interact through coupling to the zonal flows.

The authors thank the Joint Data Analysis Workshop, organized by Profs. S.-I. Itoh, S. Inagaki, and K. Itoh held at Kyushu University, Japan, and the 2nd APTWG Conference held at Southwestern Institute of Physics, China, which provided opportunities for detailed and valuable discussion on this subject. This work is supported by the National Magnetic Confinement Fusion Science Program No. 2014GB108004, No. 2013GB107001, No. 2014GB107000, and No. 2013GB112008; by the fund of State Key Laboratory of Advanced Electromagnetic Engineering and Technology in HUST (2016KF008); by the National Science Foundation of China, No. 11175060, No. 11375054, No. 91130031, and No. 11320101005; by Grant-in-Aid for Scientific Research of JSPS (15H02155, 15H02335, and 16H02442); by the Department of Energy under Award No. DE-FG02-04ER54738 and by the WCI Program of the National Research Foundation of Korea funded by the Ministry of Education, Science and Technology of Korea [WCI 2009-001].

*kjzhao@swip.ac.cn

[1] S. P. Matt, K. B. MacGregor, M. H. Pinsonneault, and T. P. Greene, Astrophys. J. **754**, L26 (2012).
[2] S. A. Balbus and J. F. Hawley, Astrophys. J. **376**, 214 (1991).
[3] S. A. Balbus and J. F. Hawley, Rev. Mod. Phys. **70**, 1 (1998).
[4] J. Aubert and A. Fournier, Nonlinear Processes Geophys. **18**, 657 (2011).
[5] D. Biskamp, *Magnetic Reconnection in Plasmas* (Cambridge University Press, Cambridge, England, 2000).
[6] P. K. Kaw, E. J. Valeo, and P. H. Rutherford, Phys. Rev. Lett. **43**, 1398 (1979).
[7] Sanae-I. Itoh, K. Itoh, and M. Yagi, Phys. Rev. Lett. **91**, 045003 (2003).
[8] T. Estrada *et al.*, Nucl. Fusion **47**, 305 (2007).
[9] Z. Lin *et al.*, in Proceedings of the 25th IAEA Fusion Conference, 2014, St. Petersburg, Russia (unpublished).
[10] T. E. Evans *et al.*, Phys. Rev. Lett. **92**, 235003 (2004).
[11] A. Hasegawa and M. Wakatani, Phys. Rev. Lett. **59**, 1581 (1987).

[12] P. H. Diamond, S.-I. Itoh, K. Itoh, and T. S. Hahm, Plasma Phys. Controlled Fusion **47**, R35 (2005).
[13] N. Winsor *et al.*, Phys. Fluids **11**, 2448 (1968).
[14] K. J. Zhao *et al.*, Phys. Rev. Lett. **96**, 255004 (2006).
[15] J. R. Robinson, B. Hnat, P. Dura, A. Kirk, and P. Tamain, Plasma Phys. Controlled Fusion **54**, 105007 (2012).
[16] K. J. Zhao *et al.*, Nucl. Fusion **55**, 073022 (2015).
[17] K. Ida *et al.*, Phys. Rev. Lett. **88**, 015002 (2001).
[18] H. Y. W. Tsui, K. Rypdal, Ch. P. Ritz, and A. J. Wootton, Phys. Rev. Lett. **70**, 2565 (1993).
[19] H. Y. W. Tsui, P. M. Schoch, and A. J. Wootton, Phys. Fluids B **5**, 1274 (1993).
[20] L. M. Pecora and T. L. Carroll, Phys. Rev. Lett. **64**, 821 (1990).
[21] A. Pikovsky, M. Rosemblum, and J. Kurths, *Synchronization: A Universal Concept in Nonlinear Sciences* (Cambridge University Press, Cambridge, England, 2001).
[22] J. A. Acebrón, L. L. Bonilla, C. J. Pérez Vicente, F. Ritort, and R. Spigler, Rev. Mod. Phys. **77**, 137 (2005).
[23] Z. B. Guo and P. H. Diamond, Phys. Rev. Lett. **114**, 145002 (2015).
[24] K. J. Zhao *et al.*, Plasma Phys. Controlled Fusion **52**, 124008 (2010).
[25] R. Jha, D. Raju, and A. Sen, Phys. Plasmas **13**, 082507 (2006).
[26] A. I. Smolyakov, A. Hirose, E. Lazzaro, G. B. Re, and J. D. Callen, Phys. Plasmas **2**, 1581 (1995).
[27] K. C. Shaing, Phys. Plasmas **9**, 3470 (2002).
[28] M. Yagi, S. Yoshida, S.-I. Itoh, H. Naitou, H. Nagahara, J.-N. Leboeuf, K. Itoh, T. Matsumoto, S. Tokuda, and M. Azumi, Nucl. Fusion **45**, 900 (2005).
[29] M. Muraglia, O. Agullo, M. Yagi, S. Benkadda, P. Beyer, X. Garbet, S.-I. Itoh, K. Itoh, and A. Sen, Nucl. Fusion **49**, 055016 (2009).
[30] M. Leconte and P. H. Diamond, Phys. Plasmas **18**, 082309 (2011).
[31] K. J. Zhao *et al.*, in Proceedings of the APTWG Meeting, Korea, 2013 (unpublished).